JCTC Journal of Chemical Theory and Computation

# Comparison of the Properties of Bent and Straight Single-Walled Carbon Nanotube Intramolecular Junctions

Bingchun Xue, Xueguang Shao, and Wensheng Cai*

*Department of Chemistry, Nankai University, Tianjin 300071, P.R. China*

Received January 21, 2009

**Abstract:** The properties of four finite-length bent and straight intramolecular junctions (IMJs) connecting two armchair and zigzag single-walled carbon nanotube segments, viz. (3,3)-(6,0) and (4,4)-(8,0), were investigated. Their structures were calculated using the density functional theory (DFT) methods at the B3LYP/6-31G(d) level of theory. The results indicate that the bent junctions are more stable than the straight ones due to the energetically favored defect structures. Remarkable differences of the HOMO and LUMO orbitals appear between the straight and the bent IMJs. The spin-unrestricted calculations at the same level of theory were also performed to obtain the antiferromagnetic-type ground state, suggesting that the spin polarizations mainly occur on the zigzag edge and the defect rings of the straight (4,4)-(8,0) IMJ and induce marked changes of the electronic structures. Additionally, the energy band structures of the four junctions with periodic boundary conditions were calculated based on DFT calculations using generalized gradient approximation with the Perdew and Wang function. The calculated band gaps suggest that the conductance of the straight IMJs is higher than the bent ones.

## Introduction

Single-wall carbon nanotubes (SWCNTs) are formed by rolling up a section of a single graphite sheet. Depending on the orientation of the roll-up vector, the SWCNTs can be metallic or semiconducting. Due to the extraordinary electronic properties, many experimental and theoretical studies have been carried out to investigate their potential use in nanoscale devices. The research has also revealed that the connections of SWCNTs with different diameter and chirality into intramolecular junctions (IMJs)[1,2] may be an important step in the development of carbon based nanoelectronic devices, because these materials are able to function as molecular diodes,[3,4] rectifiers,[5,6] electronic switches,[7,8] and so on. For the realization of nanometer-scale electronic devices, an appropriate electrical conductivity is required, which is directly related to the corresponding geometrical and electronic structures. Therefore, studies on the structures and electronic properties are important. The IMJs are generally composed of two SWCNT segments, jointed by pentagon and heptagon defects located at the interface to maintain topological consequences. The corresponding properties vary with the features of the individual segments and the amount and location of the defects at the joint part. The stabilities of the IMJs of two zigzag nanotubes and of two armchair segments have been investigated, respectively, and the most stable structures were suggested in these studies through analyzing the junctions connected by different defects.[9−11] In addition, the electronic properties of IMJs formed by different chiral tubes have also been studied theoretically,[12−15] and experimentally.[16,17] Particularly, the effect of varying the length of a metal-semiconductor IMJ on the local density of states (LDOS) was calculated.[11] In addition, for the hydrogen-terminated finite-length SWCNTs, the existence of hydrogen passivated zigzag edges has been reported to induce spin polarization on the zigzag edges.[18−21] It indicates that under the influence of an external electric field, these systems may become half-metallic with one spin channel and act as spin filters. Yet, the effect of the defects on the geometry and electronic structure and the effect of the hydrogen atoms on the spin polarization for the IMJs when joining a metallic tube to a metallic or a semiconducting tube are still fuzzy.

In this paper, the structures and band properties of the IMJs connected from armchair and zigzag nanotubes, (3,3)-(6,0)

* Corresponding author e-mail: wscai@nankai.edu.cn.

10.1021/ct900039v CCC: $40.75 
Published on Web 05/07/2009

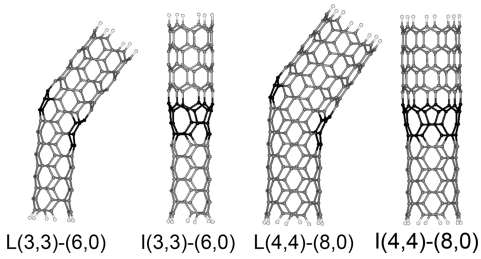


***Figure 1.*** Optimized structures of IMJs at the B3LYP/6-31G(d) theoretical level. The pentagon and heptagon rings at the joint part are visualized in black.

and (4,4)-(8,0) were investigated, respectively. Generally, all armchair and zigzag (*n*,0) (where *n* is a multiple of 3) SWCNTs are metallic. Therefore, the IMJs discussed here are considered to be a metallic-metallic and a metallic-semiconducting junction. To examine the effect of the defects, straight- and bent-shaped structures for each junction were constructed and subsequently optimized using the B3LYP/6-31G(d) method. Their stability and frontier molecular orbitals were compared. For investigation of the possible spin polarization, the calculations with the spin-unrestricted approach were also carried out. Imposing the periodic boundary conditions to the IMJ structures, their corresponding band structures were explored by means of the generalized gradient approximation (GGA) with the Perdew and Wang function (PW91). The value of the band gap may help us to understand the conductivity of these IMJs, which is important for the future application of nanoscale electric devices.

## Computational Methods

In the IMJs of (3,3)-(6,0) and (4,4)-(8,0), the corresponding two component segments in one junction have the similar diameter (4.38 ± 0.31 Å and 5.86 ± 0.44 Å). Various shaped IMJs can be formed when connecting the two segments by different position and amount of five- and seven-membered rings. In this contribution, only two typical structures, viz. bent and straight junctions, are taken into account.

The bent structures include only one pentagon and one heptagon located on the opposite position of the tube circumference. In the straight structures, the pentagons and heptagons are alternately placed on the mismatching region. According to the shape of IMJs, the bent and straight IMJs are denoted as L and I type, and four IMJs are then distinguished as L(3,3)-(6,0), I(3,3)-(6,0), L(4,4)-(8,0), and I(4,4)-(8,0), respectively, as depicted in Figure 1.

All the initially constructed structures of IMJs were optimized based on the tight binding potential for carbon. The dangling bonds at the two open ends were then saturated by hydrogen atoms in order to simulate finite nanotubes. In order to reduce the influence of the terminated hydrogen atoms on the junction region, more than three layers of carbon rings in each segment were modeled. These structures were used as starting points for the further optimization at the B3LYP/6-31G(d) theoretical level using the Gaussian 03 program packages.[22] The relative stabilities and geometric properties of IMJs were analyzed based on this level of theory.

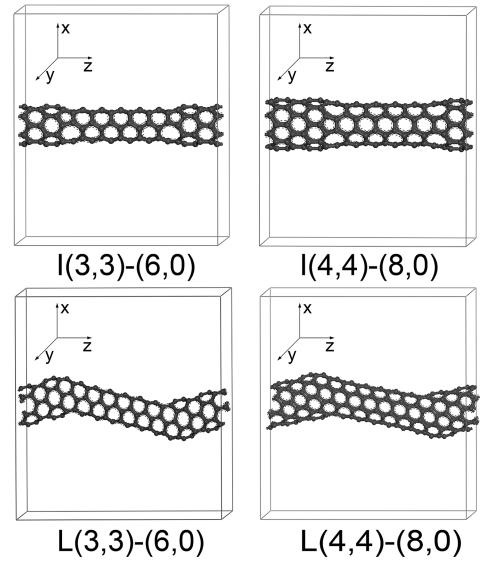


***Figure 2.*** Schematic diagram of the unit cells used to construct the infinite-length IMJs.

Due to the previous reports that spin polarization may arise from the existence of hydrogen passivated zigzag SWCNT and local structural defects,[18−21] the unrestricted B3LYP (UB3LYP) approach with the 6-31G(d) basis set was also applied to optimize the four finite-length IMJs. Since the previous studies[20,21] show that antiferromagnetic ordering is energetically favored compared to the higher spin multiplicity state, only the antiferromagnetic-type spin is calculated in this contribution. In order to obtain the antiferromagnetic-type ground state, the symmetry of the initial guess was destroyed using the Guess=(Always, Mix) keyword in the corresponding Gaussian calculations.

Moreover, to eliminate the influence of terminated hydrogen and calculate the band structures, the infinite-length IMJs were built by periodically repeating the unit cell along the *z* axis, as seen in Figure 2. Each unit cell consisted of two junction parts separated by four carbon rings to avoid the influence between each other. In the *z* direction, the length of the cell was adjusted to make the bond lengths between the atoms located in the adjacent unit cells reasonable, so that a perfect infinite-length IMJs can be obtained. In addition, in the *x* and *y* direction, a large lattice constant (35 Å for the bent and 30 Å for the straight) was applied to prevent a significant interaction between the tubes. The optimizations of the unit cells and the calculations of the band structures were performed using the Dmol$^3$ package,[23,24] which has been successfully applied to study electronic properties of carbon nanotubes.[25−27] All-electron calculations were performed with the double numerical basis set and the GGA method with PW91 function. The employed convergence criteria for structural optimizations are $1 \times 10^{-4}$ Hartree and 0.05 eV/Å for the energy and maximum displacement, respectively. Eleven Monkhorst-Pack k-points for the Brillouin zone integration along the *z* axis were used.

## Results and Discussions

**Relative Stability.** The calculation results of the four IMJs in Figure 1 using the B3LYP/6-31G(d) method are given in

***Table 1.*** Results of the Four IMJs at the B3LYP/6-31G(d) Level[a]

| | molecule | energy | HOMO | LUMO | $\Delta E$ |
|---|---|---|---|---|---|
| L(3,3)-(6,0) | $C_{114}H_{12}$ | −4350.549 | −0.152 | −0.120 | 0.032 |
| I(3,3)-(6,0) | $C_{114}H_{12}$ | −4350.496 | −0.152 | −0.133 | 0.019 |
| L(4,4)-(8,0) | $C_{156}H_{16}$ | −5954.204 | −0.148 | −0.134 | 0.014 |
| | $C_{152}H_{16}$ | −5801.732* | | | |
| I(4,4)-(8,0) | $C_{152}H_{16}$ | −5801.670 | −0.142 | −0.135 | 0.007 |

[a] $\Delta E$ is the HOMO-LUMO energy gap. All the energies are in units of Hartree. The value marked with the asterisk is calculated by the energy of $C_{156}H_{16}$ subtracting the energy of four carbon atoms.

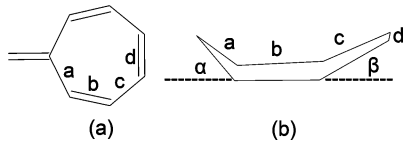


***Figure 3.*** (a) 7-Methylene-1,3,5-cycloheptatriene used as a model molecule. (b) Schematic diagram of heptagon defects in the IMJs. The labels are used to define the bonds and dihedral angles in Table 2.

Table 1. Since L(3,3)-(6,0) and I(3,3)-(6,0) possess the same number of atoms ($C_{114}H_{12}$), the relative stability can be deduced directly from their total energies, suggesting that L(3,3)-(6,0) is more stable than I(3,3)-(6,0). This method, however, is not suitable for comparison of L(4,4)-(8,0) ($C_{156}H_{16}$) and I(4,4)-(8,0) ($C_{152}H_{16}$), because of the different number of carbon atoms. Here, an alternative method was used to subtract the energy of four carbon atoms far from the defect region, which may be regarded as the atoms in the corresponding pristine tubes. To estimate the average energy of each carbon atom in the pristine (4,4) and (8,0) tubes, the energy of the same tube but with different lengths was computed, respectively. The average energy can then be obtained by the energy difference divided by the difference of the atomic numbers. To compare L(4,4)-(8,0) and I(4,4)-(8,0) with the same number of atoms, the energy of the former with 152 carbon atoms was calculated by subtracting the energy of two carbon atoms of the (4,4) tube and two of the (8,0) tubes from the original energy of L(4,4)-(8,0) with 156 carbon atoms. The computation result is marked with an asterisk in Table 1, showing that the energy of L(4,4)-(8,0) is lower than the corresponding I-IMJ, identical to the comparison result of two (3,3)-(6,0) IMJs.

**Geometric Structures.** The geometric structures of four IMJs are analyzed to explore the differences between L- and I-IMJs resulting from the different defect distribution. The results show that to accommodate the continuing lattice between two segments, the defect rings and their surrounding hexagons all have some distortions. Especially, remarkable differences are found to exist between heptagons in the different junctions. Therefore, the structures of heptagons are discussed. To coarsely estimate the distortion extent of the heptagons, the bond length and the dihedral angle of the heptagons were calculated and compared with a model molecule 7-methylene-1,3,5-cycloheptatriene shown in Figure 3a, which is a planar molecule. The results are reported in Table 2, wherein the definition of the labels involved is given in Figure 3a,b. From Table 2, it can be seen that

***Table 2.*** Distances (Å) and Dihedral Angles (°) of the Heptagon Defects in the Optimized IMJs[a]

| | a | b | c | d | α | $\beta$ |
|---|---|---|---|---|---|---|
| L(3,3)-(6,0) | 1.49 | 1.40 | 1.47 | 1.43 | 47.5 | 42.7 |
| I(3,3)-(6,0) | 1.44 | 1.43 | 1.44 | 1.42 | 11.0 | 32.2 |
| L(4,4)-(8,0) | 1.46 | 1.42 | 1.47 | 1.43 | 30.1 | 37.3 |
| I(4,4)-(8,0) | 1.43 | 1.44 | 1.43 | 1.43 | 7.0 | 26.5 |
| 7-methylene-1,3,5-cycloheptatriene | 1.47 | 1.36 | 1.45 | 1.36 | 0 | 0 |

[a] See Figure 3 for the definitions of the labels a−d, α, and $\beta$.

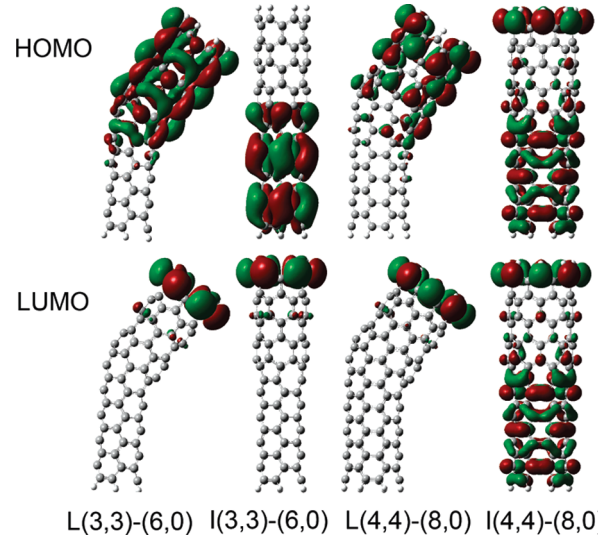


***Figure 4.*** Comparison of the HOMO and LUMO orbitals (an isovalue of 0.01 au) of the L- and I-IMJs at the B3LYP/6-31G(d) level.

compared to the model molecule the difference of the bond length of the heptagon in the L-IMJs is smaller than in the corresponding I-IMJs. The lengths of the seven bonds in the latter tend to be averaged. The distortion of the heptagons in the L-IMJs, however, is found to be more serious than in the I-IMJs by measuring the dihedral angles α and $\beta$. Apparently, although the distortion is an unfavorable factor to the stability, the number of defects in the IMJs appears to be more important, resulting in the lower energy of L-IMJs than I-IMJs.

**The Characteristic of the Frontier Molecular Orbital.** To compare the difference of the frontier molecular orbitals, the spatial distribution of the frontier molecular orbitals and the energy of the highest occupied molecular orbital (HOMO) and the lowest unoccupied molecular orbital (LUMO) were calculated. The isocontour maps of HOMO and LUMO are depicted in Figure 4. The orbital energy and the HOMO−LUMO gap ($\Delta E$) are listed in Table 1. From Figure 4, an apparent difference of HOMO distribution between L(3,3)-(6,0) and I(3,3)-(6,0) IMJs can be seen. The HOMO of the former is mainly localized on the zigzag section, whereas the HOMO of the latter is localized on the armchair section. The similar phenomenon of localization can also be found in the HOMO orbitals of L(4,4)-(8,0) and I(4,4)-(8,0), but the highest density of HOMO in I(4,4)-(8,0) appears at the zigzag edge. The uneven distribution in one junction can be ascribed to the asymmetry of the structures caused by the defects as well as different chirality, and the difference between L- and

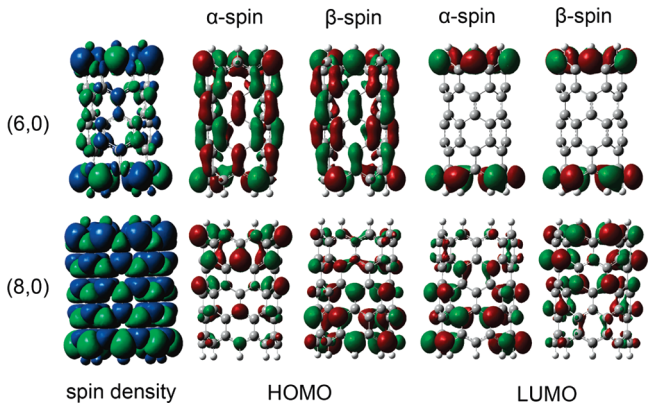


***Figure 5.*** Spin density map of the (6,0) (up left panel) and (8,0) SWCNTs (down left panel) with an isovalue of 0.004 au. Blue color for α-spin electrons, green color for $\beta$-spin electrons. α- and $\beta$-spin HOMO and LUMO orbitals of (6,0) (up) and (8,0) SWCNTs (down) with an isovalue of 0.02 au.

I-IMJs can be related to the different distribution of the defects. On the other hand, for the distribution of LUMO orbitals, differences only appear to exist between L(4,4)-(8,0) and I(4,4)-(8,0).

From the HOMO−LUMO energy gap $\Delta E$ reported in Table 1, the $\Delta E$ of L-IMJs is higher than that of the corresponding I-IMJs, indicating that the bent junctions are more stable than the straight ones, identical to the result obtained from the analysis of the total energy. Among the four IMJs, I(4,4)-(8,0) possesses the lowest energy gap, which is also reflected from the similar spatial distribution of its HOMO and LUMO shown in Figure 4.

**Spin Polarization.** To investigate the possible antiferromagnetic-type spin polarization which will probably change the electronic character of the studied systems, the calculations with the spin-unrestricted approach were carried out. For comparison, the hydrogen-terminated finite-length (6,0) and (8,0) zigzag and (3,3) and (4,4) armchair SWCNTs were also calculated using the same approach. The length of the nanotube, which is defined according to the number of carbon atoms along the tube axis, is selected to be 3.

Among the studied SWCNTs only the (6,0) and (8,0) zigzag nanotubes are found to possess a spin-polarized ground state. Nevertheless, the spin polarization phenomenon has not been observed in I(3,3)-(6,0) and L(3,3)-(6,0) junctions. According to the previous report[21] that spin polarization only appears at the end of the finite-length ($n$,0) SWCNTs when $n$ is greater than 6; therefore, it is reasonable to conjecture that only very short (6,0) CNTs present the spin-polarized state. To gain further insight into the effect of size on spin polarization, another two (6,0) and (8,0) tubes with the length of 5, same as the length of the zigzag segments in the studied junctions, were also calculated. The results show that the spin polarization only occurred in the zigzag edges of (8,0) SWCNT. As shown in Figure 5, at each side of (6,0) nanotube, the density of α- and $\beta$-spin electrons is identical; in sharp contrast, one zigzag edge of the (8,0) segment has a high density of α-spin electrons, while the other edge is rich in $\beta$-spin electrons. Moreover, the high-density α- and $\beta$-spin LUMO and HOMO orbitals

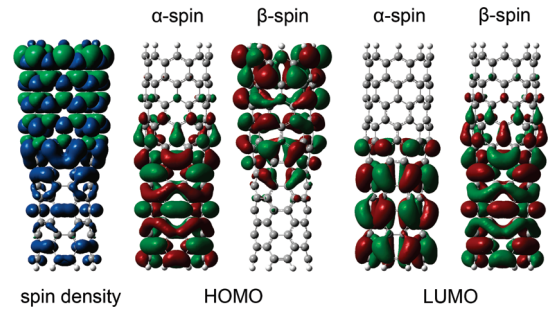


***Figure 6.*** Spin density map of the I(4,4)-(8,0) junction (left panel) with an isovalue of 0.004 au. Blue color for α-spin electrons, green color for $\beta$-spin electrons. α- and $\beta$-spin HOMO and LUMO orbitals with an isovalue of 0.01 au.

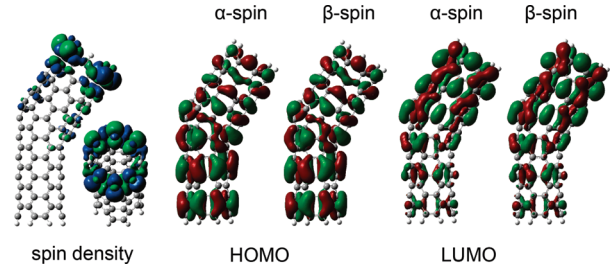


***Figure 7.*** Spin density map of the L(4,4)-(8,0) junction (left panel) with an isovalue of 0.004 au. Blue color for α-spin electrons, green color for $\beta$-spin electrons. α- and $\beta$-spin HOMO and LUMO orbitals with an isovalue of 0.01 au.

appear on the different sides of the (8,0) nanotube, whereas no difference is observed between the corresponding α- and $\beta$-spin orbitals of the (6,0) nanotube. Therefore, the dependence on the diameter and length may result in no spin-polarized ground states in (3,3)-(6,0) junctions, in which the length of the (6,0) segment is 5.

In contrast, both I(4,4)-(8,0) and L(4,4)-(8,0) present a spin polarization ground state. The spin density and the α- and $\beta$-spin LUMO and HOMO orbitals are depicted in Figure 6 for I(4,4)-(8,0) and in Figure 7 for L(4,4)-(8,0). In Figure 6, a high density of $\beta$-spin electrons is found to appear at the zigzag edge of the junction, while the α-spin electrons are mainly populated around the defect rings at the joint part. Moreover, in the entire armchair segment, the density of α-spin electrons is higher relative to $\beta$-spin electrons. It may indicate that the defects induce the spin polarization of the armchair segment. The α-spin HOMO and LUMO orbitals appear to be localized on the armchair segment of the junction. The $\beta$-spin HOMO and LUMO orbitals are found to be distributed on the zigzag and armchair segments, respectively. Interestingly, in Figure 7, a local spin polarization in L(4,4)-(8,0) only appears in the radial direction of the zigzag edge. Analysis of the HOMO and LUMO orbitals suggests no marked differences between α- and $\beta$-spin states.

Apparently, compared with Figure 4, the effect of spin polarization considerably changed the HOMO and LUMO orbitals of the (4,4)-(8,0) junctions. Whereas no changes occurred in the (3,3)-(6,0) junctions optimized using spin-unrestricted method; therefore, the orbitals are not shown.

In addition, the energies of the four IMJs optimized using the spin-unrestricted method are reported in Table 3. They

***Table 3.*** Results of the Four IMJs at the UB3LYP/6-31G(d) Level[a]

| | molecule | energy | spin | HOMO | LUMO | $\Delta E$ |
|---|---|---|---|---|---|---|
| L(3,3)-(6,0) | $C_{114}H_{12}$ | −4350.555(−0.006) | α | −0.152 | −0.120 | 0.032 |
| | | | β | −0.152 | −0.120 | 0.032 |
| I(3,3)-(6,0) | $C_{114}H_{12}$ | −4350.503(−0.007) | α | −0.152 | −0.132 | 0.020 |
| | | | β | −0.152 | −0.132 | 0.020 |
| L(4,4)-(8,0) | $C_{156}H_{16}$ | −5954.225(−0.021) | α | −0.155 | −0.121 | 0.034 |
| | | | β | −0.155 | −0.121 | 0.034 |
| I(4,4)-(8,0) | $C_{152}H_{16}$ | −5801.712(−0.042) | α | −0.152 | −0.109 | 0.043 |
| | | | β | −0.161 | −0.127 | 0.034 |

[a] $\Delta E$ is the HOMO-LUMO energy gap. All the energies are in units of Hartree. In Gaussian calculations, the Guess=(Always, Mix) keyword was used, with zero total spin. However, we encountered considerable convergence problems in optimization of I(4,4)-(8,0). Our method to circumvent the problem was to first run the calculation with the 3-21G basis set and then get the initial geometry and guess for the 6-31G(d) basis set calculation from the previous checkpoint file. In the latter calculation, the Guess=(Read, Mix) keyword was used. The energy value in the brackets is the difference between the energy in this table and the corresponding energy in Table 1.

are found to be lower than the corresponding energies using the spin-restricted method at the same level of theory. The preference for I(4,4)-(8,0) is particularly marked. It would be apparent from the table that at variance with the (3,3)-(6,0) IMJs, the spin-polarized HOMO−LUMO gap of the (4,4)-(8,0) IMJs is larger than the corresponding gap in Table 1. These indicate that the spin-polarized states are more stable than the closed shell states for the (4,4)-(8,0) junctions, in which the straight one may be detectable in experiment, and may present half-metallic behavior under the influence of an external electric field.[19−21] Moreover, the α-spin energy gap of I(4,4)-(8,0) is found to be 0.25 eV higher than the $\beta$-spin one. This phenomenon is different with the finite-length zigzag nanotubes studied in ref 21, where all the α- and $\beta$-spin energy gaps are degenerate in the absence of electric field.

**Band Structures of Infinite-Length IMJs.** From the above analysis, the existence of hydrogen and defects may induce considerable changes of the electronic properties of the finite-length IMJs studied here. To investigate the effect of the defects on the band structures in the absence of hydrogen atoms, the band structures of the infinite-length IMJs illustrated in Figure 2 have been calculated using periodic boundary conditions. For comparison purposes, the calculations of the corresponding infinite-length pristine SWCNTs have also been carried out. All the results are shown in Figure 8. Comparison of the band structures of the IMJs with the corresponding pristine tubes shows an increase of energy belts near the Fermi energy in the IMJs, which can be related to the defects in the mismatch region. The energies provided by the defect rings or the charge transfer between the different segments lead to the new states near the Fermi energy level. Furthermore, compared to I-IJMs, L-IJMs exhibit a somewhat larger band gap, in accordance with the result of the HOMO−LUMO gap of the finite-length IMJs. Band gap is related to the carrier concentration, which is one of the factors of conductivity. The higher band gaps may imply the possible lower conductivity. Accordingly, our calculations show that the straight junctions may have higher conductivity than the corresponding bent ones. Additionally, from the values of the band gaps shown in Figure 8e−h, the metallicity of the four junctions discussed here appears to have no remarkable dependence on the metallicity of the component segments.

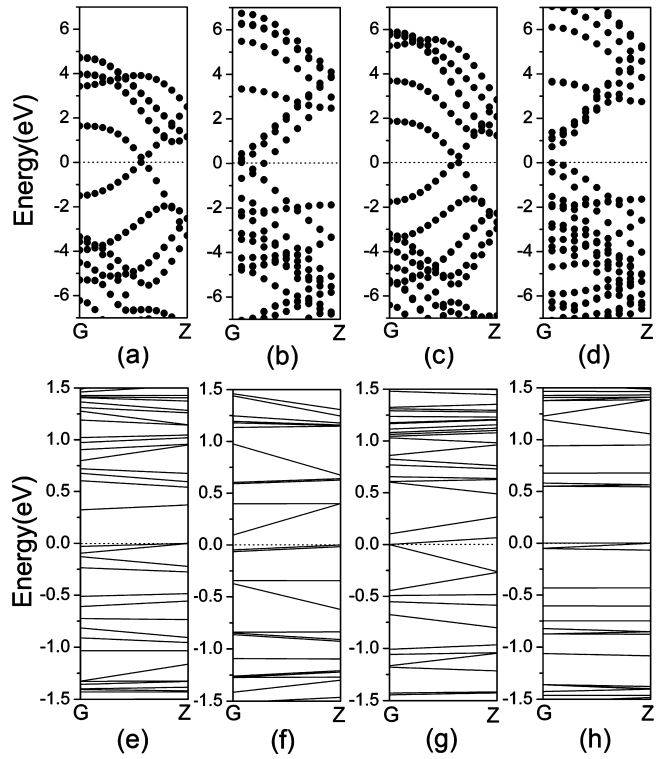


***Figure 8.*** Band structures of the infinite-length pristine SWCNT and the IMJs: (a) (3,3), metallic; (b) (6,0), metallic; (c) (4,4), metallic; (d) (8,0), semiconducting, gap, 0.72 eV; (e) L (3,3)-(6,0), gap, 0.32 eV; (f) I (3,3)-(6,0), gap, 0.10 eV; (g) L (4,4)-(8,0), gap, 0.10 eV; and (h) I (4,4)-(8,0), gap, 0.00 eV. The dashed line denotes the position of the Fermi level.

## Conclusions

Bent and straight metallic-metallic and metallic-semiconducting IMJs originating from different defect distribution were constructed and investigated. By analyzing the total energies and the HOMO−LUMO energy gaps of the IMJ structures optimized at the B3LYP/6-31G(d) theoretical level, it has been found that the bent IMJs are more stable than the corresponding straight ones. The spatial distribution of HOMO and LUMO, which is related to the trend of electron transfer, has also been calculated and compared, suggesting a distinct difference between L- and I-IMJs. The spin-polarization phenomenon was observed in the hydrogen-terminated finite-length zigzag SWCNTs but did not occur in the corresponding armchair SWCNTs, which is in agreement with the previous studies. In this contribution, the existence of hydrogen and defects is found to induce the spin polarization in the studied junctions composed of an armchair (4,4) and a zigzag (8,0) nanotube segment, particularly in the straight I(4,4)-(8,0). By analyzing the HOMO and LUMO orbitals, the effect of spin polarization is found to considerably change the electronic properties of the junctions. The spin polarization of the IMJs, however, is shown to be dependent on the diameter and length of the

zigzag segments. Furthermore, the spin-polarized ground state for the I(4,4)-(8,0) IMJ is expected to be detectable.

The effect of the defects, in the absence of the hydrogen atoms, on the band structures of the IMJs is also investigated. The band structures of the infinite-length IMJs have been calculated using periodic boundary conditions. Comparing with the corresponding pristine SWCNTs, more energy states appeared near the Fermi energy in the IMJs due to the asymmetry caused by the defects in the junctions. Moreover, different defect distributions can result in different band structures to further the effect on the conductivity of the IMJs. Our study shows that it may be possible to adjust the electronic properties of an IMJ by constructing the structure with a special defect distribution, which is important in applications.

**Acknowledgment.** This study is supported by National Natural Science Foundation of China (Nos. 20573102 and 20873066) and also supported by Nankai University ISC.

**Supporting Information Available:** Geometries of the four studied structures optimized using the B3LYP and UB3LYP with the 6-31G(d) basis set and the four infinite-length IMJs. This material is available free of charge via the Internet at http://pubs.acs.org.

## References

(1) Chico, L.; Crespi, V. H.; Benedict, L. X.; Louie, S. G.; Cohen, M. L. *Phys. Rev. Lett.* **1996**, *76*, 971–974.

(2) Liu, Y. Q.; Wei, D. C. *Adv. Mater.* **2008**, *20*, 2815–2841.

(3) Treboux, G.; Lapstun, P.; Silverbrook, K. *J. Phys. Chem. B* **1999**, *103*, 1871–1875.

(4) Lee, J. U.; Gipp, P. P.; Heller, C. M. *Appl. Phys. Lett.* **2004**, *85*, 145–147.

(5) Yao, Z.; Postma, H. W. C.; Balents, L.; Dekker, C. *Nature* **1999**, *402*, 273–276.

(6) Li, Y. F.; Hatakeyama, R.; Shishido, J.; Kato, T.; Kaneko, T. *Appl. Phys. Lett.* **2007**, *90*, 173127.

(7) Service, R. F. *Science* **1996**, *271*, 1232–1233.

(8) Li, J. Q.; Zhang, Q.; Chan-Parkb, M. B. *Carbon* **2006**, *44*, 3087–3090.

(9) Charlier, J. C.; Ebbesen, T. W.; Lambin, P. *Phys. Rev. B* **1996**, *53*, 11108–11113.

(10) Ye, Y. F.; Zhang, M. L.; Zhao, J. W.; Liu, H. M.; Wang, N. *J. Mol. Struct.: THEOCHEM* **2008**, *861*, 79–84.

(11) Garau, C.; Frontera, A.; Quinonero, D.; Costa, A.; Ballester, P.; Deya, P. M. *Chem. Phys.* **2004**, *303*, 265–270.

(12) Rochefort, A.; Avouris, P. *Nano Lett.* **2002**, *2*, 253–256.

(13) Son, Y. W.; Lee, S. B.; Lee, C. K.; Ihm, J. *Phys. Rev. B* **2005**, *71*, 205422.

(14) Wu, G.; Li, B. W. *Phys. Rev. B* **2007**, *76*, 085424.

(15) Hua, F.; Fa, W.; Dong, J. *Eur. Phys. J. B* **2005**, *46*, 331–334.

(16) Ouyang, M.; Huang, J. L.; Cheung, C. L.; Lieber, C. M. *Science* **2001**, *292*, 702–705.

(17) Shafranjuk, S. E. *Phys. Rev. B* **2007**, *76*, 085317.

(18) Kim, Y. H.; Choi, J.; Chang, K. J. *Phys. Rev. B* **2003**, *68*, 125420.

(19) Mañanes, A.; Duque, F.; Ayuela, A.; López, M. J.; Alonso, J. A. *Phys. Rev. Lett.* **2008**, *78*, 035432.

(20) Hod, O.; Scuseria, G. E. *ACS Nano* **2008**, *2*, 2243–2249.

(21) Du, A. J.; Chen, Y.; Lu, G. Q.; Smith, S. C. *App. Phys. Lett.* **2008**, *93*, 073101.

(22) Frisch, M. J.; Trucks, G. W.; Schlegel, H. B.; Scuseria, G. E.; Robb, M. A.; Cheeseman, J. R.; Montgomery, J. A., Jr.; Vreven, T.; Kudin, K. N.; Burant, J. C.; Millam, J. M.; Iyengar, S. S.; Tomasi, J.; Barone, V.; Mennucci, B.; Cossi, M.; Scalmani, G.; Rega, N.; Petersson, G. A.; Nakatsuji, H.; Hada, M.; Ehara, M.; Toyota, K.; Fukuda, R.; Hasegawa, J.; Ishida, M.; Nakajima, T.; Honda, Y.; Kitao, O.; Nakai, H.; Klene, M.; Li, X.; Knox, J. E.; Hratchian, H. P.; Cross, J. B.; Adamo, C.; Jaramillo, J.; Gomperts, R.; Stratmann, R. E.; Yazyev, O.; Austin, A. J.; Cammi, R.; Pomelli, C.; Ochterski, J. W.; Ayala, P. Y.; Morokuma, K.; Voth, G. A.; Salvador, P.; Dannenberg, J. J.; Zakrzewski, V. G.; Dapprich, S.; Daniels, A. D.; Strain, M. C.; Farkas, O.; Malick, D. K.; Rabuck, A. D.; Raghavachari, K.; Foresman, J. B.; Ortiz, J. V.; Cui, Q.; Baboul, A. G.; Clifford, S.; Cioslowski, J.; Stefanov, B. B.; Liu, G.; Liashenko, A.; Piskorz, P.; Komaromi, I.; Martin, R. L.; Fox, D. J.; Keith, T.; Al-Laham, M. A.; Peng, C. Y.; Nanayakkara, A.; Challacombe, M.; Gill, P. M. W.; Johnson, B.; Chen, W.; Wong, M. W.; Gonzalez, C.; Pople, J. A. Gaussian, Inc.: Wallingford, CT, 2004.

(23) Delley, B. *J. Chem. Phys.* **1990**, *92*, 508–517.

(24) Delley, B. *J. Chem. Phys.* **2000**, *113*, 7756–7764.

(25) Vinciguerra, V.; Buonocore, F.; Panzera, G.; Occhipinti, L. *Nanotechnology* **2003**, *14*, 655–660.

(26) Galano, A.; Orgaz, E. *Phys. Rev. B* **2008**, *77*, 045111.

(27) Bai, L.; Zhou, Z. *Carbon* **2007**, *45*, 2105–2110.

CT900039V